Desalination and Water Treatment
www.deswater.com

doi: 10.5004/dwt.2018.21905

104 (2018) 324–329
February

Grape marc activated carbon/TiO_2 hybrid degradation of RB5 azo dye: FT-IR and UV-visible analysis

Sarra Bourahla[a,*], Charef Harrats[b], Hanane Belayachi[a], Fadela Nemchi[a], Mostefa Belhakem[a]

[a]*Laboratoire de Structure, Elaboration et Application des Matériaux Moléculaires (SEA2M), Faculté des Sciences Exactes et de l'Informatique (FSEI), BP 188, Université Abdelhamid Benbadis, Mostaganem, Algeria, Tel. +213 06 62 60 56 70; emails: sarrabourahla@yahoo.fr (S. Bourahla), belayachi.hanane@hotmail.fr (H. Belayachi), delanemchi@yahoo.fr (F. Nemchi), mbelhakem@hotmail.com (M. Belhakem)*
[b]*Laboratoire de Chimie Appliquée (LAC), DGRSDT, Ctr. Univ. Bouchaib Belhadj Ain Temouchent P/284, 46000 Ain Temouchent, Algeria, email: charrats@gmail.com*

Received 10 August 2017; Accepted 13 January 2018

ABSTRACT

Activated charcoal obtained from grape marc (GMAC) was impregnated by TiO_2 anatase to form GMAC/TiO_2 hybrid. The synthesized hybrid was used in the photodegradation of reactive black 5 (RB5). The degradation products were commonly characterized from the dye solution; neglecting the traces adsorbed on the surface of the catalyst. In the present work, we targeted to follow the degradation products both on the surface of GMAC/TiO_2 hybrid by FT-IR spectroscopy and in the RB5 solution by UV-visible, after exposure to UV light during various time periods. The analysis of the hybrid surface revealed the presence of degradation species including carboxylic and sulfate groups.

Keywords: Azo dye; FT-IR; Grape marc; Hybrid; TiO_2; UV-visible

1. Introduction

Waste waters consist of a mixture of dyes, surfactants and additives that are employed during the various industrial processes [1]. Azo dyes are the largest class of colorants used in textile industry [2–7]. However, their high solubility in effluents, due to the presence of sulfonated derivatives, makes them among the major pollutants of the water discharges from textile dyes [8–11]. Some of these dyes are toxic and potentially carcinogenic [12–15].

Dye elimination from waste water is a contemporary and a crucial environmental issue. In recent years, many techniques among which adsorption are adopted for the removal of the dyes from the waste water [16]. Adsorption approach is simple and leads to high removal efficiency [9,17]. Many adsorbents including peat, silica and activated carbon (AC) have been employed for an optimal dye removal [1]. AC is one of the most widely studied adsorbent for environmental pollution control [9,18].

A second method that has been investigated for cleaning dye-containing waste water is the heterogeneous photocatalysis [5]. Among advanced oxidation processes, photocatalytic treatment allows the destruction of organic contaminants by oxidation with hydroxyl radicals (OH•) generated under mild conditions [6,7]. The technique consists of UV irradiation of semiconductors. A typical example is titanium dioxide which has been extensively studied for purification purposes thanks to its powerful oxidation strength, chemical stability, non-toxicity, low cost and good photocatalytic performance [9].

Nevertheless, the use of TiO_2 powder in a photocatalytic system is associated with several technical problems: (a) the difficulty in separating the powder from the solution after reaction is complete, (b) aggregation of particles in suspension, especially at high loadings and (c) difficulty to apply it to continuous flow systems [19,20].

* Corresponding author.

A huge volume of research work was devoted to the development of photocatalytic particle support. Systems based on alumina, zeolite, silica gel, optical fiber optic cable, glass beads, quartz, stainless steels, clays and AC were thoroughly investigated. AC is the most widely used support for heterogeneous catalysis. Over 650 open literature articles and 1,000 patents have used AC–TiO_2 mixtures or their composites [9,11,14,15,17–22].

AC provides a high surface area structure within the range of 900–1,200 m^2/g over which TiO_2 particles may be distributed and immobilized. Distribution techniques include mechanical mixing, aqueous suspensions, sol–gel, hydrothermal techniques, chemical vapor deposition, low-temperature hydrolysis, resin calcinations, microwave-assisted digestion and sonochemical methods [20].

It is also reported that the AC support plays an active part in the mechanism of photocatalysis yielding a synergistic effect between the support and the TiO_2 particles [23–25].

The combination of the two systems offers the following advantages:

1. Regeneration can be conducted in-situ that enables to reduce time and energy spent in removal and transport of materials.
2. The thermal regeneration energy is conserved and no loss in carbon volume or porosity occurs.
3. The pollutant and photocatalyst are intimately brought in direct contact on the surface of the carbon. In contrast to the solution process, the photocatalyst is spontaneously available.
4. Toxic intermediates formed during pollutant degradation are also re-adsorbed onto the carbon surface and are subsequently oxidized.

The purpose of this study is to permeate by TiO_2 anatase, at room temperature, an activated charcoal obtained from grape marc (GMAC). The resulting hybrid (GMAC/TiO_2) is used in the photodegradation of reactive black 5 (RB5). To our knowledge in the literature, the products resulting from the photodegradation were searched for in the solution of the degraded dye [5,6]. The traces that might adsorb on the surface of the photocatalyst were not considered. In the present work, we considered both the solution of RB5 and the surface of the hybrid. The former was analyzed using UV-visible spectrophotometer, whereas the products adsorbed on the surface of the GMAC/TIO_2 were characterized using FT-IR spectroscopy. These analyses were carried out at different times of UV degradation, viz. 15, 30, 45 and 60 min.

2. Materials and methods

2.1. Materials

The titanium dioxide, TiO_2, was mainly anatase (99.7%). According to the manufacturer's specifications [26], the elementary particle in dry powder form was approximately spherical in shape having an average particle size of 25 nm. The specific surface area was within a range of 200–220 $m^2\ g^{-1}$, in agreement with the manufacturer's specification.

AC was prepared from grape seeds provided from the cavern of Sidi M'Hamed Ben Ali (Relizane, Algeria). Absolute ethanol was produced in France (PROLABO). Other chemical reagents used were of analytical grade.

2.2. Preparation of activated carbon

In a typical experiment, grape seeds were washed several times with distilled water, dried at 100°C overnight, crushed and 140 μm sieved. The resulting material was then impregnated in 40% phosphoric acid solution for 2 h. The obtained suspension was filtered off and then the impregnated material was dried at 110°C for 24 h. The activation of dried impregnated grape marc leaves was performed in a muffle furnace at 600°C at a heating rate of 10°C min^{-1} for 3 h.

The residue was washed in 0.1 N hydrochloric acid solution, followed by repeated washing with laboratory-produced hot distilled water until the filtrate was free from phosphate ions as confirmed by conductivity measurements and lead acetate tests. The prepared AC was dried at 100°C for 24 h, ground and sieved to obtain an average particle size of <71 μm. This material was noted activated grape marc (GMAC).

2.3. Preparation of photocatalyst hybrid

TiO_2/GMAC was prepared by agitating 1 g of activated carbon (GMAC) in 10 mL of 1 M phosphoric acid solution. 24 h later 0.1 g of titanium dioxide TiO_2 was added to the solution. The obtained suspension was stirred mechanically at room temperature for 8 h. The impregnated powder was recovered by filtration and successive washing with distilled water until a neutral pH is obtained. A further washing with ethanol was necessary to eliminate any traces of water before the material was dried at 105°C. The preparation of the AC and the hybrid was described in more details elsewhere [21].

2.4. Dye

The azo dye, Reactive Black 5 (color index 306452), is used in the dying industry for coloring silk. It was provided by Sigma-Aldrich (USA) and used without further purification. Synthetic test dye solutions were prepared by dissolving accurate amount of RB5 in distilled water and subsequently diluting to required concentrations [21]. Some molecular characteristics of RB5 in non-hydrolyzed form are listed in Table 1. Fig. 1 shows the chemical structure of the azo dye.

2.5. Photocatalytic degradation

The photocatalytic activity was studied by degrading the RB5 dye as a target pollutant [25]. The experiments were conducted in a black box plated by mirrors to ensure both complete irradiation with UV light and isolation in darkness. The irradiation tests were carried out in a 50 mL cylindrical glass reactor equipped with an ultraviolet (UV) lamp (VL-215.L 2×15W-365nm tube, power 60 W, made in France). The lamp was placed horizontally using 25 mL of RB5 solution with an initial concentration of 100 μM. After adsorption equilibrium was reached in the dark, the light was turned on to irradiate the solution. The first blank sample was taken at time zero ($t_0 = 0$) [26]. The dye decolorization was analyzed as follows:

$$\text{Dye discoloration} = \frac{(C_{\text{dye},t_o} - C_{\text{dye},t})}{C_{\text{dye},t_o}} \times 100 \quad (1)$$

Table 1
Selected physical and chemical characteristics of the RB5 dye

Name	Reactive Black 5 (diazo)
Synonyms	Remazol Black B
Class	Anionic
Empirical formula	$C_{26}H_{21}N_5O_{19}S_6$
Molecular weight (g/mol)	991.81
λ_{max}	595 nm

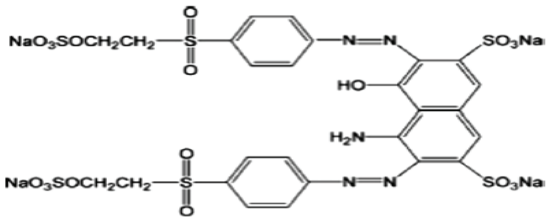

Fig. 1. Chemical structure of RB5.

where $C_{dye,t}$ and C_{dye,t_0} are the concentrations of the dye at reaction time t and $t_0 = 0$, respectively.

2.6. UV-visible analysis

Samples of the dye solution were withdrawn during the course of the reaction at periodic intervals and analyzed in a UV-visible scanning spectrum 300–700 nm, using a UV-visible spectrophotometer. The color of the dye solution in the reaction mixture at different times was obtained by measuring the absorbance at maximum wavelength (λ_{max} = 595 nm) and by computing the concentration from a calibration curve [3].

2.7. FT-IR study

The FT-IR spectra were recorded after different durations of exposure to UV light on an IR-Prestige 21 Fourier transform spectrometer (Shimadzu, Japan) at 2 cm^{-1} resolution in the wavelength range 4,000–400 cm^{-1}. To make the pellets, 0.05 mg of samples were mixed with 100 mg of potassium bromide (KBr) then compressed under a pressure of 1 GPa.

3. Results and discussions

3.1. Study of absorption spectra

The decolorization of the aqueous solution of RB5 (100 μmol/L) is followed by UV-visible spectroscopy before and after treatment by UV lamp (Fig. 2). Prior to treatment, the spectra of the aqueous solution of RB5 consist of two absorption bands at 310 and 595 nm. The absorption peak at 595 nm can be assigned to a chromophore containing a long conjugated π system linked by two azo groups [3]. The absorption peak at 310 nm can be attributed to the naphthalene component which is bound to the transition π → π* [27,28]. In addition, two sources of nitrogen including azo and amine groups linked to a naphthalene ring are present in RB5.

When 100 μmol/L of RB5 solution in contact with 0.05 g of TiO_2/GMAC was irradiated by UV lamp at different time intervals, it was clearly observed that the intensity of absorption peak in the visible region (595 nm) disappears very fast after few minutes of exposure. The UV band at 310 nm was also observed to vanish but at a lower rate than the visible band. The OH• radicals first attacks the azo groups and opens the N=N bonds. The long conjugated π systems are destructed leading to decolorization. Second, since N=N bonds are easier to disrupt than aromatic ring structures, the elimination of adjacent ring structure requires longer time.

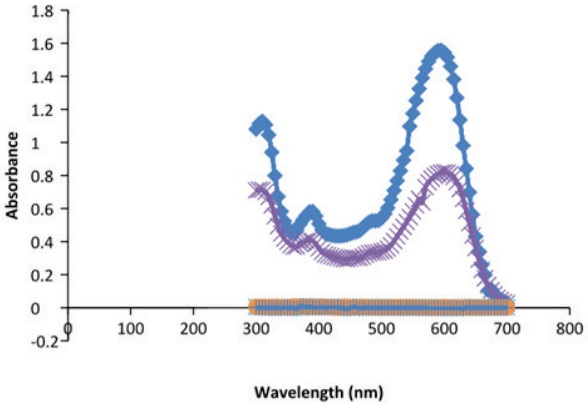

Fig. 2. UV-visible spectra of the RB5 dye at different time periods: 0 ( ), 15 ( ), 30 ( ), 45 ( ) and 60 min ( ).

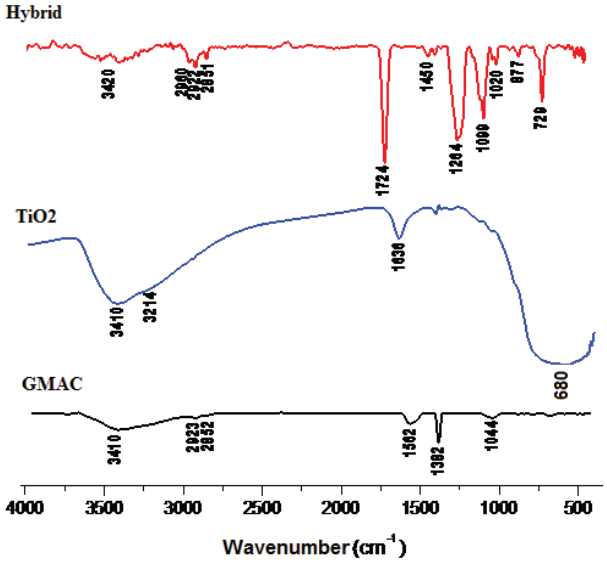

Fig. 3. FT-IR transmission spectra: GMAC, hybrid, TiO_2 anatase.

3.2. FT-IR structural analysis

3.2.1. Surface state of the materials

FT-IR analysis was carried out on GMAC, TiO_2 and hybrid individual materials for a comparison purpose (Fig. 3).

The FT-IR spectra of the prepared samples inform us on the vibrational state of the functional groups accessible on the surface of the materials [29,30].

Interpretation of the FT-IR spectrum of grape marc AC:

- 3,410 cm^{-1}: this band is ascribed to the stretching vibration of the alcohol or eventually phenol OH groups
- 2,923 and 2,852 cm^{-1} are associated to the symmetrical and asymmetrical stretching vibrations of the methyl group of an alkane, respectively
- 1,562 cm^{-1} is a characteristic band of the stretching vibration of C=C link of an aromatic cycle
- The strong band at 1,382 cm^{-1} results from the angular deformation of methyl and/or hydroxyl groups.
- 1,044 cm^{-1} band is caused by the stretching vibration of P–O–P in polyphosphate, or the ionized P^{+}–O^{-} bond in the ester of phosphate acid [31,32].

The spectrum of TiO_2 anatase contains a stretching vibration band at 3,410 cm^{-1} and a deformation at 1,636 cm^{-1} assigned to O–H bond (Ti–OH) resulting from the presence of water traces. The band visible at 3,214 cm^{-1} is assigned to the stretching vibration of adsorbed water molecules on Ti ($Ti–OH_2$) [33]. The intense absorption bands extending within 450–750 cm^{-1} range are due to combined vibration modes of the Ti–O–Ti bond [34]. The spectrum of the hybrid precursor presents a series of characteristic bands, the assignments of which are gathered in Table 2.

The FT-IR spectrum of RB5 colorant is shown in Fig. 3. The characteristic absorption bands and their assignments are gathered in Table 3.

3.2.2. FT-IR spectra before and after degradation

FT-IR spectroscopy in transmission mode has been used to elucidate the chemical reactions occurring on the surface of GMAC/TiO_2 hybrid. The evolution during time of the FT-IR traces of the hybrid upon exposition to UV light is presented in Fig. 4.

The absorption band situated at 3,396 cm^{-1} is assigned to the stretching vibration of Ti–OH of the hybrid precursor [32]. Upon UV irradiation of the hybrid surface, the intensity of this band is consequently reduced. Fig. 4 illustrates the variation of the band intensity as a function of the irradiation time. Furthermore, the stretching vibration absorption bands of the methyl group appearing at 2,960; 2,922 and 2,851 cm^{-1} vanish after 60 min of UV irradiation time. In the region of 2,000–450 cm^{-1}, the stretching vibration bands of C=O visible at 1,724 and 1,264 cm^{-1} disappear after 15 min of irradiation exposure. New absorption bands associated with the stretching vibration of sulfates and carboxylates anions appeared at 1,428 and 1,386 cm^{-1}, respectively [36].

The disappearance of the absorption bands within the range of 1,500–1,450 cm^{-1} initially present in the RB5 dye indicates clearly that no more azo bonds and aromatic ring survive the exposure to the UV irradiation process. The persistence, after 30 min of UV exposure, of the stretching vibration absorption band of the aromatic –C=C– bonds at 1,547 cm^{-1}, although its intensity diminished, proves that the degradation of the aromatic cycle was slower compared with that of –N=N– bonds. Note that the stretching vibration of Ti–O visible within 750–500 cm^{-1} range reveals that the active carbon remains impregnated with anatase even after 60 min of degradation time.

The increase in the intensity of the absorption band at 1,383 cm^{-1}, associated with the formation of sulfates and carboxylates, translates an increase of the amount of these degradation products. After 60 min of irradiation time a characteristic absorption band of –CO carboxylic acid appeared at 1,134 cm^{-1}.

Fig. 5 shows the relative intensities of the peaks corresponding to the SO_4^{-}, COO^{-} and S=O for the hybrid after irradiation at different time periods. The figure reveals that the degradation products including the sulfates, the carboxylates and the S=O groups do not evolve beyond 15 min of UV irradiation time.

4. Conclusion

TiO_2 anatase deposited on activated grape marc carbon with impregnation/mixing method shows a good adhesion and photocatalytic activity.

Table 2
FT-IR absorption bands of the hybrid precursor

Absorption band (cm^{-1})	Assignment
3,420	Stretching vibration of O–H of an intermolecular alcohol and/or of the $Ti–OH_2$ bond resulting from adsorbed water molecules
3,100–3,000	Associated to the =C–H elongation vibration of aromatic cycle
2,960; 2,922; 2,851	Weak intensity bands associated to the symmetrical and the asymmetrical stretching vibrations of the methyl group of an alkane
1,724	Strong intensity band; stretching vibration of C=O carbonyl group
1,450	Weak intensity band; stretching vibration of alkane C–C bond
1,264; 1,099	Symmetrical and asymmetrical stretching vibrations of C–O bond of carboxylic acid, respectively
1,020	Weak intensity band; stretching vibration of P–O–P in polyphosphates or ionized P^{+}-O^{-} bond in acid phosphate ester
877	Stretching vibration assigned to Ti–O–C; this band translates a strong interaction between Ti–O and the activated carbon [34]
729	Weak to medium intensity band; stretching vibration of Ti–O; this band confirms the impregnation of the activated carbon with anatase [35]

Table 3
Assignment of the characteristic peaks of RB5 spectrum

Frequencies (cm^{-1})	Intensity	Assignment
3,500–3,200	Large and strong band	Characteristic of O–H elongation vibration bonded to an alcohol and/or N–H elongation vibration of amine
3,100–3,000	Shoulder	Associated to the =C–H elongation vibration of aromatic cycle
2,928	Average	Associated to the symmetrical C–H elongation vibration of CH_2 group
2,865	Average	Associated to the asymmetrical elongation vibration of CH_2 group
1,635	Strong	Attributed to the C=N elongation vibration
1,600–1,450	Strong	Characteristics to the C = C elongation vibration of aromatic cycle
1,381	Average to weak	Associated to the C–C elongation vibration of alkane
1,340–1,250	Strong	Associated to the C–N elongation vibration of aromatic amine
1,350–1,330	Strong	Characteristics of the S=O elongation vibration of sulfonated group
1,126	Strong	Associated to the S=O elongation vibration of sulfonated group
1,000–769		Various elongations S–O–C
800–765	Average to strong	Associated to the = C–H deformation vibration of aromatic cycle
614		Associated to the elongation vibration of the SO_4 group

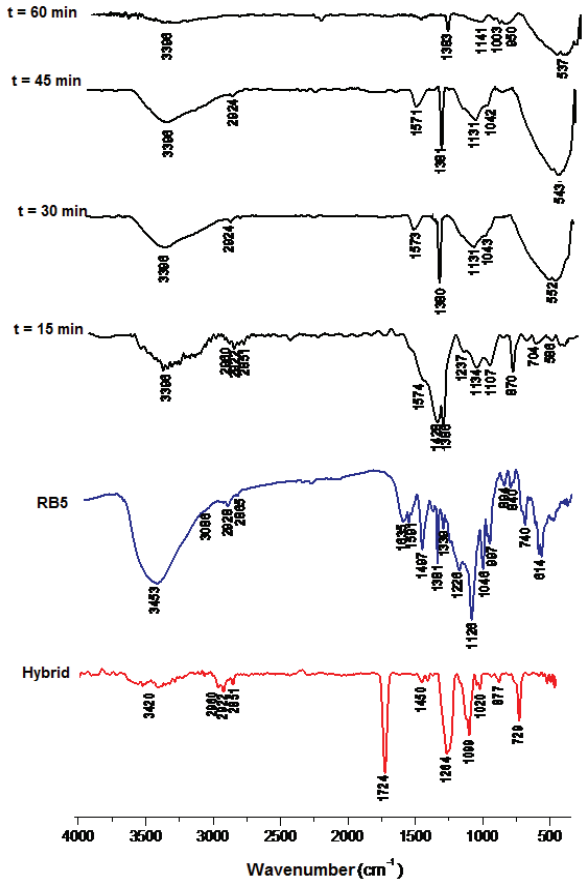

Fig. 4. FT-IR spectra of the hybrid, RB5 and irradiated hybrid at different time periods.

The photocatalytic activity has been verified via UV-visible spectroscopy. The formation of sulfate ions and the cleavage of the –N=N– azo groups were observed.

FT-IR spectroscopy allowed us to demonstrate that the concentrations of C=O, C–H and C–C absorbing at 1,724; 2,960; 1,020 cm^{-1}, respectively, decrease as a function of the UV

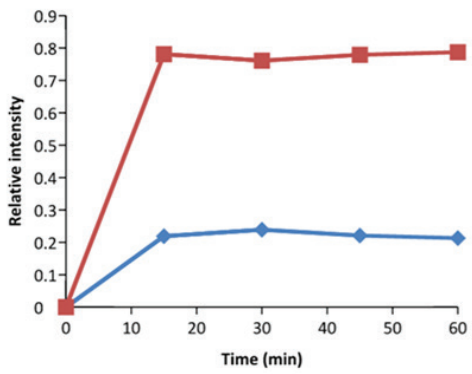

Fig. 5. Relative intensities of the IR bands of the SO_4^-, COO^- ( ) and S=O ( ) for the hybrid after irradiation at different time periods.

irradiation exposure time. The oxidizing action results from the degradation of the chromophore part of the RB5 molecule. The colorant degradation products including sulfates and carboxylates were successfully revealed by FT-IR analysis.

References

[1] A.Y. Khan, Titanium Dioxide Coated Activated Carbon: A Regenerative Technology for Water Recovery, MSc Thesis, University of Florida, 2003.
[2] G. Moussavi, M. Mahmoudi, Removal of azo and anthraquinone reactive dyes from industrial wastewaters using MgO nanoparticles, J. Hazard. Mater., 168 (2009) 806–812.
[3] S.Y. Yang, X. Yang, X.T. Shao, R. Niu, L.L. Wang, Activated carbon catalyzed persulfate oxidation of azo dye acid orange 7 at ambient temperature, J. Hazard. Mater., 186 (2011) 659–966.
[4] C. Cai, Z.Y. Zhang, J. Liu, N. Shan, H. Zhang, D.D. Dionysiou, Visible light-assisted heterogeneous Fenton with $ZnFe_2O_4$ for the degradation of orange II in water, Appl. Catal., B, 182 (2016) 456–668.
[5] S. Garcia-Segura, E. Brillas, Combustion of textile monoazo, diazo and triazo dyes by solar photoelectro-Fenton: decolorization, kinetics and degradation routes, Appl. Catal., B, 181 (2016) 681–191.

[6] A.M.S. Solano, S. Garcia-Segura, C.A. Martínez-Huitle, E. Brillas, Degradation of acidic aqueous solutions of the diazo dye congo red by photo-assisted electrochemical processes based on Fenton's reaction chemistry, Appl. Catal., B, 168 (2015) 559–971.
[7] F.C. Moreira, S. Garcia-Segura, V.J.P. Vilar, R.A.R. Boaventura, E. Brillas, Decolorization and mineralization of sunset yellow FCF azo dye by anodic oxidation, electro-Fenton, UVA photoelectro-Fenton and solar photoelectro-Fenton processes, Appl. Catal., B, 142 (2013) 877–790.
[8] Z. Aksu, Application of biosorption for the removal of organic pollutants: a review, Process Biochem., 40 (2005) 997–1026.
[9] M.N. Chong, V. Vimonses, S.M. Lei, B. Jin, C. Chow, C. Saint, Synthesis and characterisation of novel titania impregnated kaolinite nano–photocatalyst, Microporous Mesoporous Mater., 117 (2009) 233– 242.
[10] M. Dias, M.C.M. Alvim-Ferraz, M.F. Almeida, J. Rivera-Utrilla, M. Sanchez-Polo, Waste materials for activated carbon preparation and its use in aqueous-phase treatment: a review, J. Environ. Manage., 85 (2007) 833–846.
[11] D. Huang, Y. Miyamoto, T. Matsumoto, T. Tojo, T. Fan, J. Ding, Q. Guo, D. Zhang, Preparation and characterization of high–surface–area TiO_2/activated carbon by low–temperature impregnation, Sep. Purif. Technol., 78 (2011) 9–15.
[12] A.K. Gupta, A. Pal, C. Sahoo, Photocatalytic degradation of mixture of Crystal Violet (Basic Violet 3) and Methyl Red dye in aqueous suspensions using Ag^+ doped TiO_2, Dyes Pigm., 69 (2006) 224–432.
[13] M.S. Lucas, J.A. Peres, Decolorization of the azo dye reactive Black 5 by Fenton and photo-Fenton oxidation, Dyes Pigm., 71 (2006) 236–644.
[14] J.M. Peralta-Hernandez, J. Manrıquez, Y. Meas-Vong, F.J. Rodrıguez, T.W. Chapman, M.I. Maldonado, L.A. Godınez, Photocatalytic properties of nano-structured TiO_2-carbon films obtained by means of electrophoretic deposition, J. Hazard. Mater., 147 (2007) 588–593.
[15] N. Remya, J.G. Lin, Current status of microwave application in wastewater treatment, Chem. Eng. J., 166 (2011) 797–713.
[16] J. Matos, A. Garcia, L. Zhao, M.M. Titirici, Solvothermal carbon-doped TiO_2 photocatalyst for the enhanced methylene blue degradation under visible light, Appl. Catal., A, 390 (2010) 175–182.
[17] Y.H. Ao, J.J. Xu, D.G. Fu, X.W. Shen, C.W. Yuan, Low temperature preparation of anatase TiO_2-coated activated carbon, Colloid Surf., A, 312 (2008) 125–130.
[18] J. Xu, Y. Ao, M. Chen, D. Fu, C. Yuan, Photocatalytic activity of vanadium-doped titania–activated carbon composite film under visible light, Thin Solid Films, 518 (2010) 4170–4174.
[19] D. Huang, Y. Miyamoto, J. Ding, J. Gu, S. Zhu, Q. Liu, T. Fan, Q. Guo, D. Zhang, A new method to prepare high-surface-area N–TiO_2/activated carbon, Mater. Lett., 65 (2011) 326–628.
[20] R. Leary, A. Westwood, Carbonaceous nanomaterials for the enhancement of TiO_2 photocatalysis, Carbon, 49 (2011) 741–172.
[21] H. Belayachi, B. Bestani, N. Benderdouche, M. Belhakem, The use of TiO_2 immobilized into grape marc-based activated carbon for RB-5 Azo dye photocatalytic degradation, Arab. J. Chem., in press.
[22] Z. Bouberka, A. Khenifi, N. Benderdouche, Z. Derriche, Removal of Supranol Yellow 4GL by adsorption onto Cr-intercalated montmorillonite, J. Hazard. Mater., B133 (2006) 154–461.
[23] H.K. Son, S. Sivakumar, M.J. Rood, B.J. Kim, Electrothermal adsorption and desorption of volatile organic compounds on activated carbon fiber cloth, J. Hazard. Mater., 301 (2016) 27–34.
[24] G.B. Baur, I. Yuranov, L. Kiwi-Minsker, Activated carbon fibers modified by metal oxide as effective structured adsorbents for acetaldehyde, Catal. Today, 249 (2015) 252–258.
[25] X. Wang, Y. Liu, Z. Hu, Y. Chen, W. Liu, G. Zhao, Degradation of methyl orange by composite photocatalysts nano-TiO_2 immobilized on activated carbons of different porosities, J. Hazard. Mater., 169 (2009) 1061–1067.
[26] A. Aguedach, S. Brosillon, J. Morvan, L. El Kbir, Photocatalytic degradation of azo-dyes reactive black 5 and reactive yellow 145 in water over a newly deposited titanium dioxide, Appl. Catal., B, 57 (2005) 55–62.
[27] I. Gultekin, N.H. Ince, Degradation of aryl-azo-naphthol dyes by ultrasound, ozone and their combination: effect of R-substituents, Ultrason. Sonochem., 13 (2006) 208–214.
[28] H.E. Zhong, Y. Shaogui, J.U. Yongming, S. Cheng, Microwave photocatalytic degradation of Rhodamine B using TiO_2 supported on activated carbon: mechanism implication, J. Environ. Sci., 21 (2009) 268–872.
[29] H.Y. Chen, O. Zahraa, M. Bouchy, F. Thomas, J.Y. Bottero, Adsorption properties of TiO_2 related to the photocatalytic degradation of organic contaminants in water, J. Photochem. Photobiol., A, 85 (1995) 179–986.
[30] S. Xu, J. Ng, X. Zhang, H. Bai, D. Delai-Sun, Adsorption and photocatalytic degradation of Acid Orange 7 over hydrothermally synthesized mesoporous TiO_2 nanotube, Colloids Surf., A, 379 (2011) 169–175.
[31] J. Matos, J. Laine, J.M. Herrmann, Effect of the type of activated carbons on the photocatalytic degradation of aqueous organic pollutants by UV irradiated titania, J. Catal., 200 (2001) 10–20.
[32] P.A. Connor, K.D. Dobson, A.J. McQuillan, Infrared spectroscopy of the TiO_2/aqueous solution interface, Langmuir, 15 (1999) 2402–2408.
[33] Z. Li, B. Hou, Y. Xu, D. Wu, Y. Sun, Hydrothermal synthesis, characterization, and photocatalytic performance of silica-modified titanium dioxide nanoparticles, J. Colloid Interface Sci., 288 (2005) 149–154.
[34] C.H. Zhou, S. Xu, Y. Yang, B.C. Yang, H. Hu, Z.C. Quan, B. Sebo, B.L. Chen, Q.D. Tai, Z.H. Sun, X.Z. Zhao, Titanium dioxide sols synthesized by hydrothermal methods using tetrabutyl titanate as starting material and the application in dye sensitized solar cells, Electrochim. Acta, 56 (2011) 4308–4314.
[35] L.F. Liu, P.H. Zhang, F.L. Yang, Adsorptive removal of 2,4-DCP from water by fresh or regenerated chitosan/ACF/TiO_2 membrane, Sep. Purif. Technol., 70 (2010) 354–361.
[36] X.Q. Gong, A. Selloni, A. Vittadini, Density functional theory study of formic acid adsorption on anatase TiO_2(001): geometries, energetics, and effects of coverage, hydration, and reconstruction, J. Phys. Chem. B, 110 (2006) 2804–2811.